ChemPubSoc Europe

DOI: 10.1002/cssc.201601272

CHEMSUSCHEM Full Papers

Synergistic Effect of Cobalt and Iron in Layered Double Hydroxide Catalysts for the Oxygen Evolution Reaction

Fengkai Yang,[a] Kirill Sliozberg,[b] Ilya Sinev,[c] Hendrik Antoni,[a] Alexander Bähr,[a] Kevin Ollegott,[a] Wei Xia,[a] Justus Masa,[b] Wolfgang Grünert,[a] Beatriz Roldan Cuenya,[c] Wolfgang Schuhmann,[b] and Martin Muhler*[a]

Co-based layered double hydroxide (LDH) catalysts with Fe and Al contents in the range of 15 to 45 at% were synthesized by an efficient coprecipitation method. In these catalysts, Fe^{3+} or Al^{3+} ions play an essential role as trivalent species to stabilize the LDH structure. The obtained catalysts were characterized by a comprehensive combination of surface- and bulk-sensitive techniques and were evaluated for the oxygen evolution reaction (OER) on rotating disk electrodes. The OER activity decreased upon increasing the Al content for the Co- and Al-based LDH catalysts, whereas a synergistic effect in Co- and Fe-based LDHs was observed, which resulted in an optimal Fe content of 35 at%. This catalyst was spray-coated on Ni foam electrodes and showed very good stability in a flow-through cell with a potential of approximately 1.53 V at 10 mA cm^{-2} in 1 M KOH for at least 48 h.

Introduction

In the last decade, water electrolysis, which converts intermittently available renewable energy into H_2, has drawn a lot of attention owing to the increasing global energy demand.[1] Its key challenge is the high overpotential required to reach the solar flux equivalent current density (e.g., 10 mA cm^{-2}), which mainly results from the sluggish oxygen evolution reaction (OER) as a result of its four-electron-transfer pathway.[1,2] For this reason, suitable OER catalysts have to be applied to lower the overpotential, which thereby increases the water oxidation efficiency. Materials such as RuO_2 and IrO_2 are known to be the most active OER catalysts under acidic conditions.[3] However, their scarcity and high costs limit their application on a large scale. In comparison, Co-based materials are known to be promising OER catalysts in alkaline electrolytes and are thus more appealing for large-scale use because of their high abundance on earth and the low cost of cobalt.[4]

To study the nature of self-assembled Co-based OER active centers, numerous efforts have been undertaken focusing on cobalt phosphate (Co–Pi) catalysts electrodeposited from a phosphate-containing electrolyte.[5–10] It is widely accepted that Co–Pi catalysts consist of amorphous hydrated cobaltates mainly in the Co^{3+} oxidation state as deposited and partly in the Co^{4+} state under the reaction conditions.[5,7,10] Further structural studies indicate that Co–Pi catalysts are built of fragments containing CoO_6 octahedra,[6] which are further assembled in the form of a layered structure intercalated with anions.[8,9,11] For heterogeneous Co-based OER catalysts, however, conflicting conclusions have been reported. Yeo and Bell[12] suggested that the OER activity should be promoted by $Co^{3+/4+}$ sites on the basis of their study of a gold-supported thin layer of Co_3O_4. In contrast, it was independently reported by Bao et al.[13] and Xu et al.[14] that the OER activity was improved by oxygen vacancies in Co_3O_4 nanosheets with Co in a lower oxidation state. These conflicting findings can become compatible if a recently proposed mechanism is taken into account for which it is assumed that active species on Co_3O_4 surfaces are formed in situ and that tetrahedral Co^{2+} sites are more suitable than octahedral Co^{3+} sites in a Co_3O_4 spinel structure for the formation of active species under working conditions.[15] Similar to Co–Pi catalysts, the in situ formed OER-active species on Co-based heterogeneous catalysts consist of hydrated cobaltate fragments in a layered structure.[16,17] Until now, hydrated cobaltates have been detected under working conditions by means of different in situ techniques on the surfaces of various Co-based heterogeneous catalysts, including

[a] F. Yang, H. Antoni, A. Bähr, K. Ollegott, Dr. W. Xia, Prof. Dr. W. Grünert, Prof. Dr. M. Muhler
Laboratory of Industrial Chemistry
Ruhr-University Bochum
Universitätsstr. 150
D-44780 (Germany)
E-mail: muhler@techem.rub.de

[b] Dr. K. Sliozberg, Dr. J. Masa, Prof. Dr. W. Schuhmann
Analytical Chemistry and Center for Electrochemical Sciences (CES)
Ruhr-University Bochum
Universitätsstr. 150
D-44780 (Germany)

[c] Dr. I. Sinev, Prof. Dr. B. R. Cuenya
Department of Physics
Ruhr-University Bochum
Universitätsstr. 150
D-44780 (Germany)

Supporting Information and the ORCID identification number(s) for the author(s) of this article can be found under http://dx.doi.org/10.1002/cssc.201601272.

This publication is part of a Special Issue celebrating "10 years of ChemSusChem". To view the complete issue, visit: http://dx.doi.org/10.1002/cssc.v10.1.

perovskite,[18] phosphate salt,[16] CoO,[17] and Co_3O_4.[19] Thus, studies on both electrodeposited Co–Pi and Co-based heterogeneous catalysts point to the dependence of the intrinsic OER activity on Co (oxy)hydroxides in layered structures.

Layered double hydroxides (LDHs) consist of positively charged layered hydroxide sheets formed by tilted edge-sharing MO_6 octahedra and negatively charged counterions (e.g., NO_3^-, CO_3^{2-}, etc.) in the interlayers. Therefore, LDHs have the closest structural similarity to the in situ formed Co-based OER-active species. Recently, Boettcher and co-workers[20] observed a synergistic effect between Co and Fe by electrodepositing a series of hydroxides with different Co/Fe ratios, which is consistent with other work on electrodeposited CoFe-based LDHs showing that the presence of Fe ions significantly promotes the activity of Co-based LDH OER catalysts.[21,22] However, it is difficult to precisely control the Co/Fe ratio in electrochemically deposited thin-film catalysts because of the differing deposition kinetics. In this work, we synthesized CoFe- and CoAl-based LDH catalysts with Fe and Al contents in the range of 15 to 45 at% by an efficient coprecipitation method. In these catalysts, the Fe^{3+} or Al^{3+} ions play an essential role as trivalent species to stabilize the LDH structure. The obtained catalysts were characterized by a comprehensive combination of surface- and bulk-sensitive techniques and were evaluated for OER activity on rotating disk electrodes (RDEs). The OER activity decreased upon increasing the Al content for the CoAl-based LDH catalysts, whereas a synergistic effect in the CoFe-based LDHs was observed for an optimal Fe content of 35 at%. This catalyst was spray-coated on Ni foam electrodes and was tested for long-term stability; it showed very good stability with a potential of approximately 1.53 V versus reversible hydrogen electrode (RHE) at 10 mA cm^{-2} in 1 M KOH for at least 48 h.

Results and Discussion

Four CoAl and five CoFe LDH catalysts were prepared in varied Co to Al/Fe ratios by coprecipitation at pH 9 by using a 2 M/0.3 M $NaOH/Na_2CO_3$ solution as the precipitating agent (see the Experimental Section for more details), which was followed by drying at room temperature and grinding in a mortar. The obtained catalysts were designated as CoAl*m* and CoFe*n*, with *m* and *n* as the Al and Fe atomic contents, respectively. As summarized in Table S1 (Supporting Information), the Co and Al/Fe contents were quantified by inductively coupled plasma optical emission spectrometry (ICP-OES). Generally, the determined Al and Fe contents were consistent with the nominal values of both the CoAl and CoFe LDHs, which thus demonstrated the complete coprecipitation of Co^{2+} and Al^{3+}/Fe^{3+} ions at pH 9. In some of the samples, small differences between the nominal and experimentally determined Al/Fe contents (max. 0.85 at%) were observed, which were attributed to experimental errors during the synthesis.

The obtained samples were characterized by X-ray diffraction (XRD) to determine the dependence of the structural properties on the Al/Fe content. As shown in Figure 1a, all CoAl LDH samples exhibit reflections at approximately $2\theta =$ 11.5 and 23°, which are the characteristic (003) and (006) reflections of the $Co(OH)_2$ LDH structure.[23] Each reflection can be assigned to the reference pattern of the pure $Co(OH)_2$ LDH, which indicates that the LDH is the only crystalline product. A closer look at the patterns of the CoAl LDHs reveals that all of the CoAl LDH samples possess slightly higher 2θ values between 11.5 and 11.9° relative to the (003) reflection at $2\theta =$ 11.0° in the reference pattern, which indicates a smaller interlayer distance between the hydroxide layers in the CoAl LDHs. Interestingly, the 2θ values of the (003) reflection in the CoAl LDHs increases gradually from 11.5 to 11.9° with higher Al contents above 25 at%. This observation can be attributed to a smaller interlayer distance, which may result from the larger fraction of Al^{3+} ions with smaller ionic radii in the hydroxide layer and the stronger electronic attraction between more positively charged hydroxide layers with higher Al contents and counteranions in the interlayer. In addition, the CoAl15 and CoAl45 samples have a significantly higher full width at half maximum (FWHM) of the reflections than the other samples with medium Al contents, which demonstrates that smaller crystalline domains are formed with either too high or too low Al^{3+} concentrations. Thus, the LDH structure cannot be sufficiently stabilized with low Al^{3+} concentrations, whereas high Al^{3+} concentrations lead to disordered LDH hydroxide layers

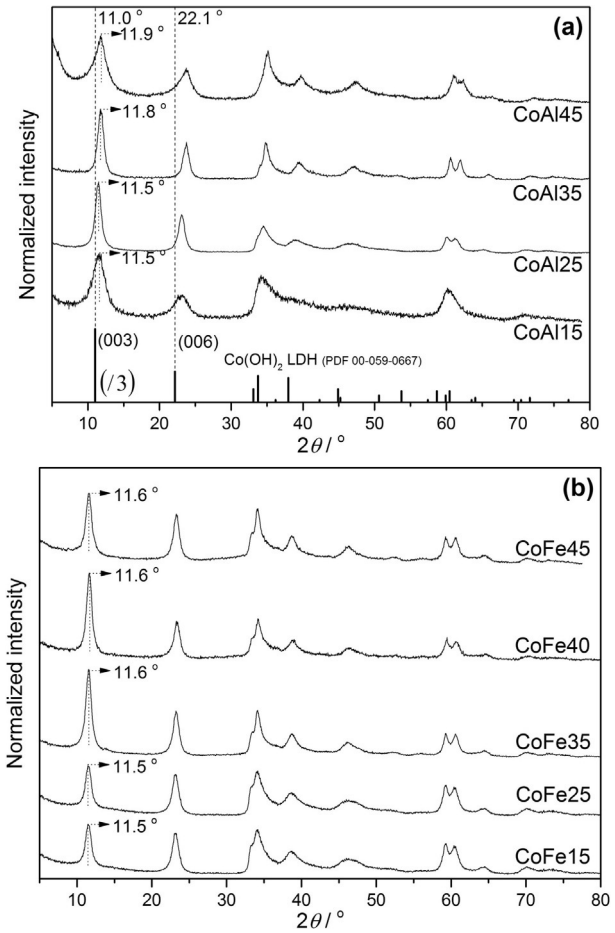

Figure 1. XRD patterns of the a) CoAl and b) CoFe samples with varied Co^{2+} to M^{3+} ratios.

presumably as a result of the different radii of the Co^{2+} and Al^{3+} ions. Similar to the CoAl LDHs, the CoFe samples exhibit the typical patterns of LDH structures for Fe contents between 15 and 45 at% (Figure 1b). Upon increasing the Fe content, the (003) reflections are shifted slightly to higher 2θ values from 11.5 to 11.6°. Unlike the CoAl samples, the CoFe LDHs show much smaller changes in both the 2θ and FWHM values upon increasing the Fe content, which is attributed to the more similar ionic radii of the Co and Fe ions in the hydroxide layer. Therefore, the CoFe LDHs can be formed with a good crystalline structure with less disorder over a wide range of Fe concentrations.

The Raman spectra of the CoAl and CoFe LDHs are displayed in Figure 2. As shown in Figure 2a, the asymmetric band at a shift of 476 cm^{-1} and the most intense band at 521 cm^{-1} are observed for the CoAl samples. It has been reported that similar bands occur at shifts of 462 and 521 cm^{-1} for a hydrotalcite-like CoAl LDH[24] and at shifts of 457 and 523 cm^{-1} for brucite-like $Co(OH)_2$.[25] Pérez-Ramírez et al.[24] assigned the two bands to hydroxy groups mainly associated with Al, and both bands were influenced by probably one divalent cation in its coordination. In contrast, Yang et al.[25] assumed that the two bands were correlated with the Co–O symmetric stretching and O–Co–O bending modes, respectively. In this work, upon increasing the Al content, the band at a shift of 476 cm^{-1} decreases dramatically, which leaves small symmetric bands, and the band at a shift of 521 cm^{-1} almost disappears. These observations suggest that the band at a shift of 476 cm^{-1} can be assigned to the hydroxy groups coordinated to Al^{3+}, whereas the band at 521 cm^{-1} and the band at approximately 450 cm^{-1}, which slightly overlaps with the band at 476 cm^{-1}, are correlated with hydroxy groups bound to Co^{2+} and are strongly influenced by its coordination. In addition, another band is observed at a shift of 1057 cm^{-1} for the CoAl LDHs, and it is assigned to OH bending vibrations.[24,25] Similar to the CoAl LDHs, the CoFe samples show symmetric bands at shifts of 454 and 521 cm^{-1} for low Fe contents (Figure 2b). Upon increasing the Fe content, both bands decrease significantly and are hardly observed if the Fe content is above 30 at%. This finding confirms the assignments of the bands at shifts of 454 and 521 cm^{-1} to the hydroxy vibrations of the CoFe LDHs, which is in good agreement with the observations made for the CoAl LDHs. Interestingly, the band at a shift of 1057 cm^{-1} is barely detected in any of the CoFe LDH samples. Given that one HO^- anion is shared by three $Co(OH)_6$ octahedra in a $Co(OH)_2$ layer,[9] the Raman bands at 454 and 521 cm^{-1} actually originate from HO^- groups bound to 3 Co^{2+} cations. This configuration is statistically rarely formed with an Al^{3+} or Fe^{3+} content of more than 33 at%, which leads to a significant decrease in the Raman intensities of the bands at shifts of 454 and 521 cm^{-1} for the CoM35, CoM40, and CoM45 samples.

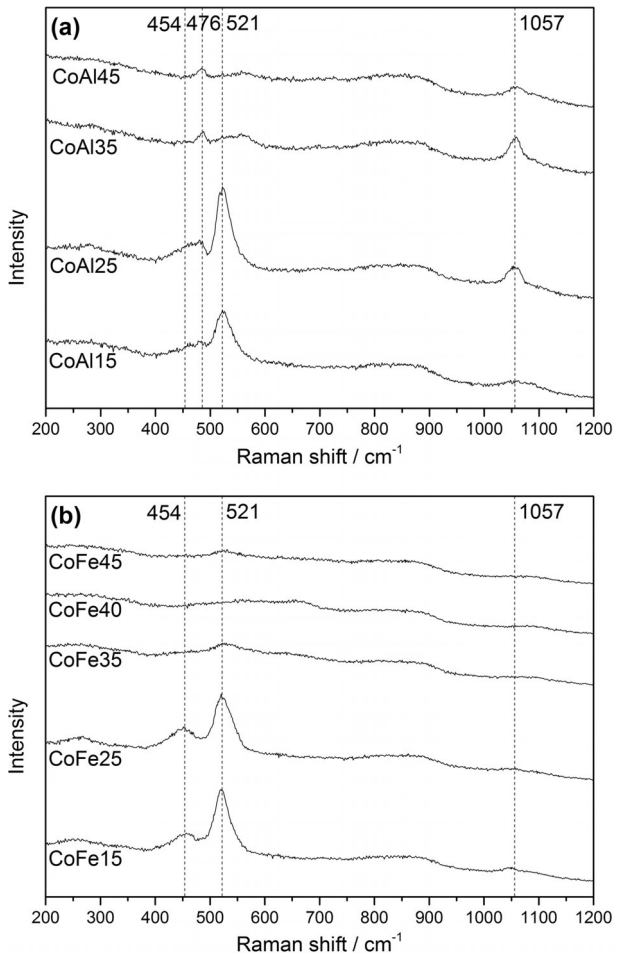

Figure 2. Raman spectra of the a) CoAl and b) CoFe samples with varied Co^{2+} to M^{3+} ratios.

The thermal decomposition of the CoAl35 and CoFe35 LDHs was studied by thermogravimetric mass spectrometry (TG-MS). As shown in Figure 3a, CoAl35 undergoes significant decomposition in 5 vol% O_2/He above 50 °C and shows one small shoulder at $T = 92$ °C and two intense peaks at $T = 172$ and 242 °C in the differential thermogravimetric analysis (DTG) profile, which are in good agreement with reported TG studies on CoAl LDH.[24,26] Taking the MS profiles into account, the DTG peak at $T = 172$ °C is correlated to the release of H_2O ($m/z = 18$) at 185 °C, whereas the DTG peak at $T = 242$ °C is due to the formation of both H_2O and CO_2 ($m/z = 44$) at approximately 250 °C. In comparison, the CoFe35 sample decomposes upon heating, which results in three intense DTG peaks at $T = 147$, 185, and 393 °C (Figure 3b). The MS profiles show that the most intense mass loss at $T = 147$ °C originates from dehydration with a strong $m/z = 18$ signal at 155 °C. The mass loss peak at $T = 185$ °C results mainly from the release of both H_2O ($m/z = 18$) at 189 °C and CO_2 ($m/z = 44$) at 199 °C. The mass loss at $T = 393$ °C, which is only observed for CoFe35, can be assigned to either the decomposition of NO_3^- with significant formation of NO ($m/z = 30$) at 375 °C or the thermal decomposition of $Co_{0.65}Fe_{0.35}O_x$ containing Fe^{3+} to the $FeCo_2O_4$ spinel containing Fe^{2+}, which leads to the release of O_2. The latter speculation is supported by the observation that a lower temperature is observed for the third DTG peak upon heating CoFe35 in pure He (Figure S1).

The temperature-programmed reduction (TPR) profiles of the CoAl and CoFe LDHs are displayed in Figure 4. The CoAl LDHs are hardly reduced up to 300 °C, and in the temperature range

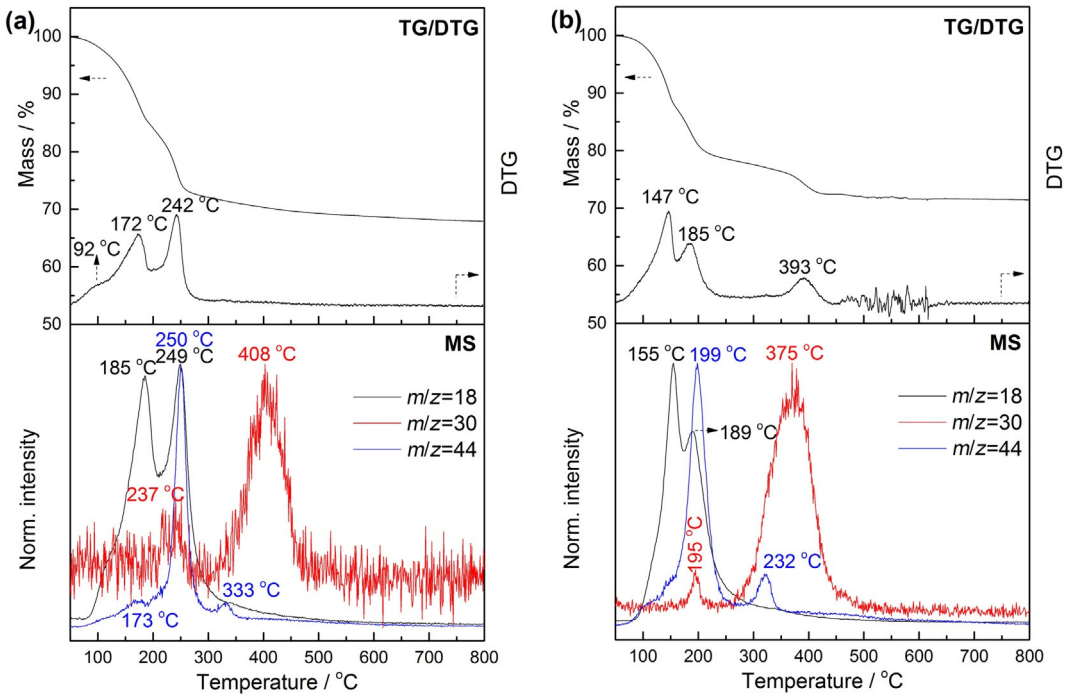

Figure 3. TG-MS profiles of the a) CoAl35 and b) CoFe35 samples at a heating rate of 5 K min^{-1} to 800 °C in 5 vol% O_2/He.

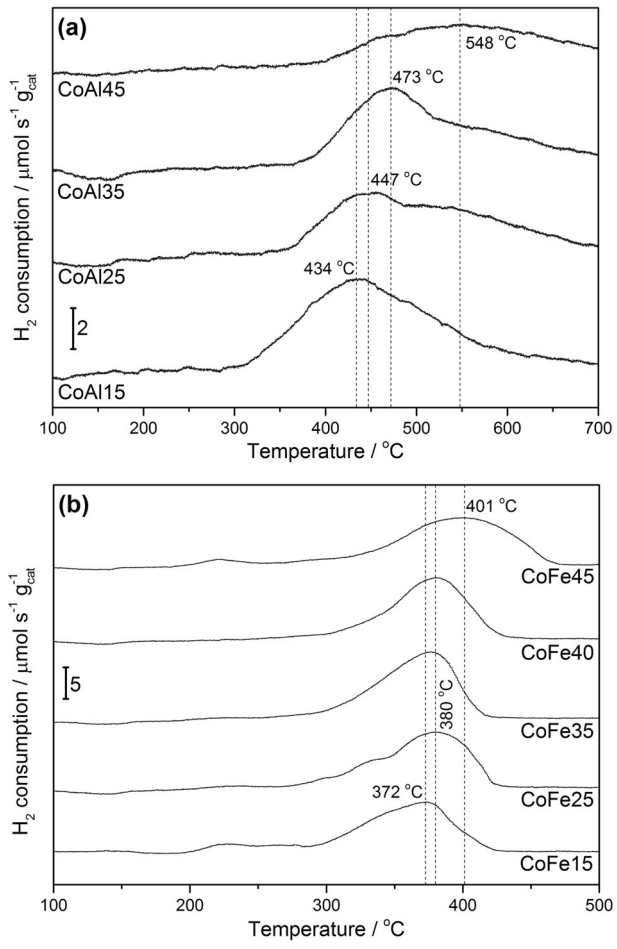

Figure 4. TPR profiles of the a) CoAl and b) CoFe samples with varied Co^{2+} to M^{3+} ratios.

of 300 to 700 °C only broad and weak H_2 consumption peaks are detected. This observation is consistent with the reported TPR profiles of noncalcined CoAl LDHs, for which the presence of the Al^{3+} ions led to incomplete reduction of Co^{2+}.[27] Upon increasing the Al content, the H_2 consumption peak is shifted to higher temperature from 434 °C for CoAl15 to 548 °C for CoAl45, which demonstrates the detrimental effect of a higher Al content on the reducibility of Co. In comparison, the CoFe samples show more defined reduction profiles between 300 and 500 °C. The H_2 consumption maximum is gradually shifted from approximately 372 to 401 °C upon increasing the Fe content. However, the individual reduction of the Co and Fe ions cannot be distinguished in the TPR profiles. The shift in the H_2 consumption peak is in good agreement with the reported TPR profiles of bimetallic $CoFeO_x$, which showed that the reduction temperature of FeO_x was higher than that of CoO_x.[28] Taking the TG-MS study into account, which monitored strong dehydration and decarboxylation processes below 250 °C, the main H_2 consumption by CoAl and CoFe LDHs in the TPR profiles between 300 and 500 °C most probably results from the reduction of oxide species mixed with anions formed by thermal decomposition.

The X-ray photoelectron (XP) spectra of selected CoFe LDHs were recorded and are displayed in Figure 5. In the C 1s spectra, aliphatic and carbonate species are detected at binding energies (BEs) of 284.5 and 288.6 eV, respectively (Figure 5 a). CO_3^{2-} was introduced to stabilize the LDH structure as a counteranion in the interlayers. The deconvoluted O 1s spectra consist of two oxygen species at BE = 529.3 and 530.9 eV, which can be assigned to oxide-like and hydroxide-like oxygen species, respectively (Figure 5 b).[20] In addition, the spectra of the oxide-like oxygen species increases significantly at higher Fe contents, which confirms the correlation between the Fe^{3+}

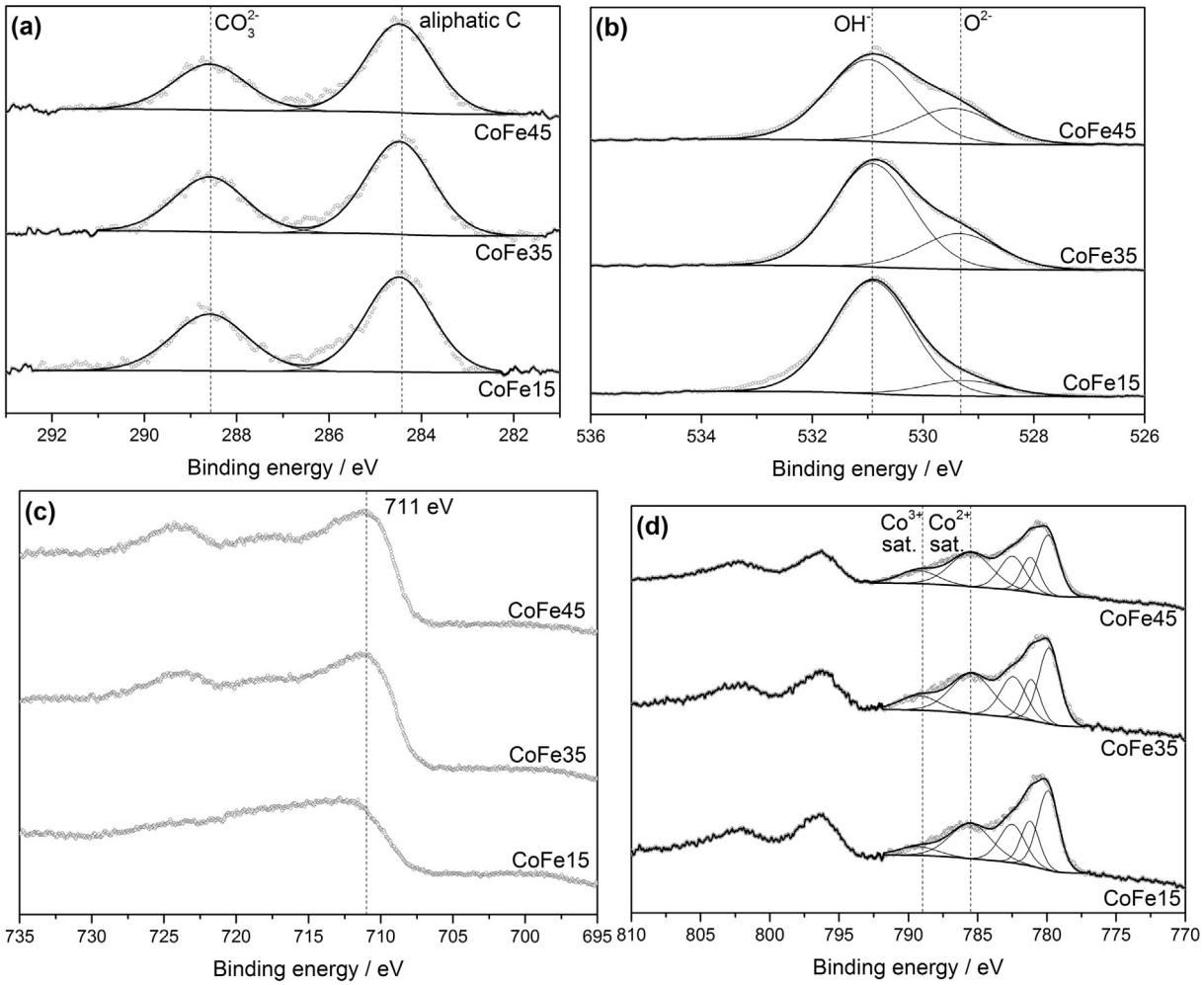

Figure 5. XP spectra of a) C 1s, b) O 1s, c) Fe 2p, and d) Co 2p of selected CoFe samples.

and O^{2-} species. The Fe 2p spectrum with a maximum at BE = 711 eV is similar to the previously reported spectra of FeOOH (Figure 5 c).[29] The Co 2p spectra do not change with varied Fe contents. The intense satellite at BE = 785.2 eV indicates that the Co species are mainly in the Co^{2+} oxidation state.

To obtain more insight in the local coordination geometry of the metal ions, X-ray fine structure absorption spectroscopy (XAFS) was performed by using selected CoFe LDHs at both the Fe and Co *K* absorption edges. The Fe-*K* X-ray absorption near edge structure (XANES) spectra do not change with different Fe/Co ratios, which shows a pre-edge feature at 7113.8 eV, an intense band above the edge at 7132.6 eV (so-called white line, WL) and two features in the postedge region at approximately 7139.9 and 7148.4 eV (Figure S2 a). The overall shape of the XANES spectra does not follow any of those of the reference iron oxides (Figure S3 a). The pre-edge peak position and intensity, however, indicate a dominance of Fe^{3+} species in sixfold coordination according to the pre-edge features of crystalline Fe^{2+}- and Fe^{3+}-containing compounds as observed by Wilke et al.[30] A similar shape of the Fe-*K* XANES spectra was recently reported for mixed NiFe oxyhydroxides.[31,32] Similar to the FeK edge, the CoK edge XANES spectra show only insignificant differences (Figure S2 b). By comparing them to reference spectra (Figure S3 b), it can be concluded that Co is dominantly in the Co^{2+} state, which is consistent with the Co 2p XP spectra.

Additional results on FeK edge and CoK edge extended X-ray absorption fine structure (EXAFS) spectra of the selected CoFe LDHs are displayed in Figure 6. At both edges, the spectra are dominated by intense backscattering features at r = 1.45/1.62 Å (FeK and CoK edge, respectively, not corrected for phase shift) and at r = 2.69 Å (uncorrected), which likely correspond to metal-to-oxygen and metal-to-metal backscattering in a hydroxide structure. It is particularly remarkable that the intensity of the metal-to-metal feature in the Fe-*K* EXAFS decreases upon increasing the iron content, whereas the intensity changes in the first peak assigned to Fe–O are less strong but follow the same trend. In contrast, there is no well-defined trend in the CoK edge EXAFS spectra, with more intense features observed for the CoFe35 sample.

To obtain a deeper understanding of the local coordination of Co^{2+} and Fe^{3+}, EXAFS spectra were fitted by using structural models built by using the orthorhombic $Co(OH)_2$ structure,[33] in which Co^{2+} and Fe^{3+} occupy equal crystallographic positions with an atomic ratio of 1:1 (Figures S4 and S5). For each spectrum, M–O and M–M (M = Fe, Co) shells were fitted. An at-

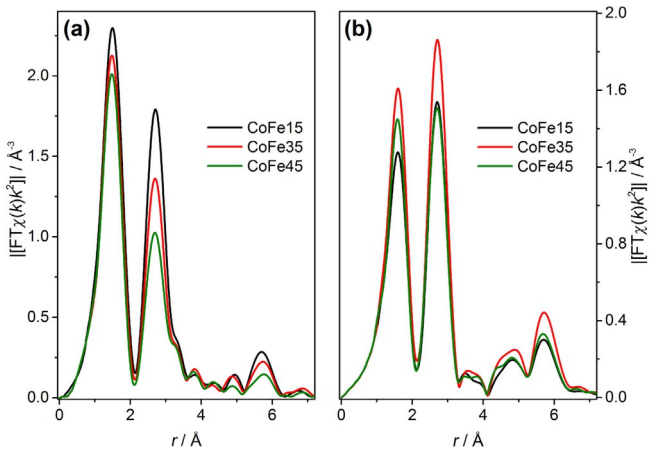

Figure 6. a) FeK and b) CoK edge EXAFS spectra of CoFe15, CoFe35, and CoFe45.

tempt was made to fit the feature at $r = 2.69$ Å with both M–Fe and M–Co coordination, but owing to the close atomic numbers of Co and Fe, unreasonable results were obtained. Thus, the Fe–O coordination number (CN) changes from approximately 5.8 to 5.5 upon increasing the iron content from 15 to 35 at% and further to approximately 5.2 for the sample with 45 at% Fe, whereas the Fe–M CN undergoes more significant changes from approximately 5.0 to 4.2 and finally to approximately 3.9 (see Table S2 for details). The best model fit of the CoK edge EXAFS spectra shows that the highest Co–O and Co–M CNs for the CoFe35 sample are 4.57 and 7.67, respectively (see Table S3), whereas the other two samples share close Co–M CNs of 7.35 and 7.26 for CoFe15 and CoFe45, respectively. This analysis seems to suggest that the Fe^{3+} ions may prefer to be located at the edges of the LDH platelets upon increasing the Fe content, whereas the Co^{2+} ions might be located more in the center of the platelets.

The OER activities of the CoAl and CoFe LDHs were determined by drop-coating a suspension of the catalysts on glassy carbon rotating disc electrodes (GC RDEs, 3.8 mm diameter) to form thin films. As shown in Figure 7a, the OER activity decreases upon increasing the Al content from 15 to 45 at%, which corresponds to an increase in the potential at 10 mA cm^{-2} from 1.63 to 1.68 V versus RHE, respectively; this indicates that the presence of Al^{3+} ions suppresses the OER activity by diluting the Co sites in the CoAl LDHs. Another possible explanation for the diminished activity upon increasing the Al content can be an effective drop in the charge-transfer rate through the catalyst bulk. Considering redox-hopping-type conduction and the presence of mixed $Co^{2+/3+}$ valencies,[34] insertion of electrochemically inactive Al^{3+} ions in the crystal lattice disables redox hopping, and the minimal distance for an electron to overcome would be the distance between two Co ions separated by an Al^{3+} ion. Given that this distance is much larger than that between two adjacent Co ions, the charge-transfer rate drops in accordance with the Marcus theory.[35] In contrast to Al^{3+}, Fe^{3+} is a redox-active species that can participate in the redox-hopping-type charge transfer along with Co. The CoFe LDHs show much better OER activities than the CoAl LDHs with potentials at 10 mA cm^{-2} between 1.58 and 1.68 for all of the samples. The activity first increases upon increasing the Fe content up to 35 at% Fe and then decreases with any further increase in the Fe content. Thus, an optimal Fe content of 35 at% is derived for the CoFe LDHs (Figure 7b).

The Tafel plots follow trends similar to those of the polarization curves. As shown in Figure 7c, the Tafel slopes increase continuously from 64 mV dec^{-1} for CoAl15 to approximately 83 mV dec^{-1} for CoAl25 and CoAl35, and finally to 102 mV dec^{-1} for CoAl45. In contrast, the Tafel slopes of the CoFe LDHs decrease significantly from 70 mV dec^{-1} for CoFe15 to 49 mV dec^{-1} for CoFe35, and then further decrease slightly to 47 mV dec^{-1} for CoFe45 (Figure 7d). The overpotentials at 10 mA cm^{-2} and Tafel slopes of the CoAl and CoFe LDHs are summarized in Figure 7e. Both the overpotentials at 10 mA cm^{-2} and the Tafel slopes of the CoAl catalysts increase upon rising the Al content. Although the presence of Al^{3+} is necessary to maintain the LDH structure, it appears that the sites occupied by Al^{3+} do not participate in the OER. Instead, such sites inhibit the reaction owing to substitution of the catalytically active Co sites. In contrast, the CoFe catalysts exhibit a volcano-like plot in both the overpotentials at 10 mA cm^{-2} and the Tafel slopes as a function of the Fe content in the catalysts. The optimal Fe content is approximately 35 at%, which suggests a synergistic interaction between the Fe and Co ions during the OER.

Table 1 summarizes the OER activities reported in the literature; they demonstrate that the results obtained with the optimized LDH CoFe35 catalyst presented in this work are comparable or even better than most published OER results for Co LDH-related catalysts.

The long-term stability of the optimal CoFe35 catalyst was further investigated under conditions closer to application by a galvanostatic stability (GSS) test[40] in a flow-through cell at a current density of 10 mA cm^{-2}. The catalyst was deposited on a Ni foam electrode (1.0 × 1.0 cm^2) by means of spray-coating with an optimized sample loading of 4.5 mg cm^{-2}. As shown in Figure 8, the ohmic drop (*iR*)-corrected potential applied to the working electrode at 10 mA cm^{-2} is plotted as a function of time. The potential during polarization of the electrode at 10 mA cm^{-2} first decreases slightly from approximately 1.50 V

Table 1. Comparison of the electrocatalytic performance of CoFe35 with Co LDH-related catalysts reported in the literature.

Sample[a]	Current density[b] [V vs. RHE]	Tafel slope [mV dec^{-1}]	Electrolyte	Ref.
CoFe35 LDH	1.58	49	0.1 M KOH	this work
CoZn LDH	≈1.72[c]	–	0.1 M KOH	[36]
exfol. Co LDH	1.58	45	1 M KOH	[37]
CoMn LDH	1.55	43	1 M KOH	[38]
CoFe LDH film	–	29	1 M KOH	[20]
CoO/Co_3O_4 nc	1.66	89	0.5 M KOH	[17]
LDH FeCo	1.56	85	1 M KOH	[39]
gelled FeCoW	1.45	37	1 M KOH	[39]

[a] Exfol.: exfoliated; nc: nanocubes. [b] At 10 mA cm^{-2}. [c] Converted from the raw data based on the normal hydrogen electrode.

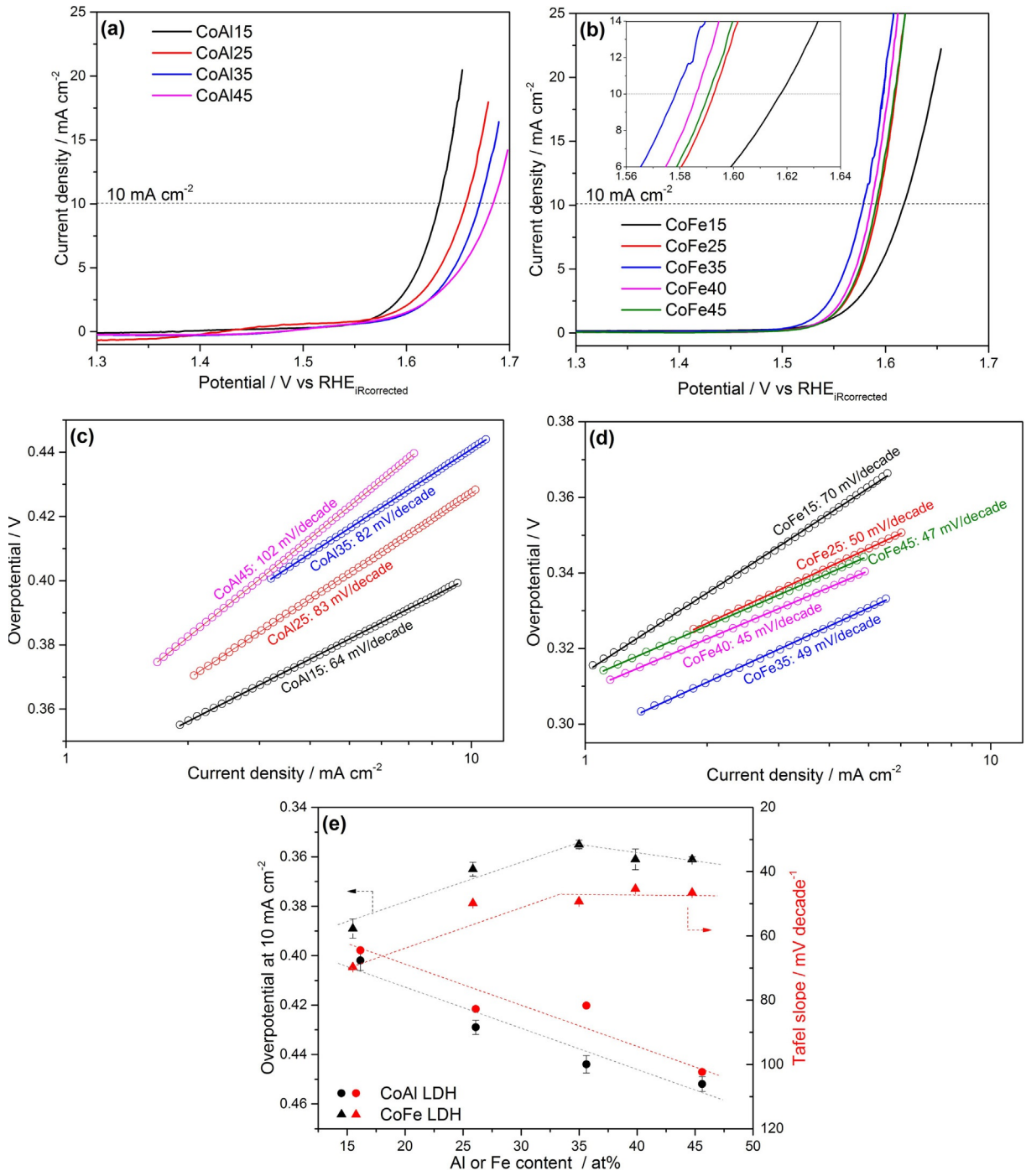

Figure 7. OER activities of the a) CoAl and b) CoFe samples; Tafel slopes of the c) CoAl and b) CoFe samples; e) overpotential at 10 mA cm^{-2} and Tafel slopes of the catalysts versus Al/Fe atomic content, as determined by ICP-OES.

versus RHE in the first 1 h and then increases to approximately 1.51 V versus RHE after 5 h. After that, it suddenly increases to approximately 1.53 V versus RHE, which is probably due to detachment of a part of the catalyst film from the electrode. Interestingly, after the initial deactivation processes within the first 5 h, thereafter the catalyst generally maintains stable performance with only minor fluctuations at approximately 1.53 V versus RHE. The changes in the ambient temperature contribute to the fluctuations in the potential curve in accordance with the diurnal cycle. In general, the CoFe35 catalyst exhibits very good stability in the OER in an alkaline electrolyte for at least 48 h.

It is widely accepted that the incorporation of Fe dramatically improves the OER activity of Ni-based LDH catalysts.[31,32,41,42] Trotochaud et al.[41] showed that pure Ni-LDH catalysts without Fe exhibited very poor OER activity, and more importantly, Fe was found to be the only promising dopant exhibiting a synergistic effect on Ni among several redox-active metals.[42]

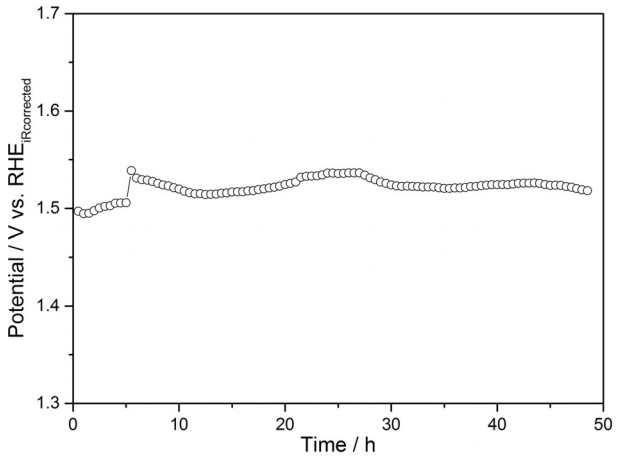

Figure 8. Long-term stability of CoFe35 during continuous polarization at 10 mA cm^{-2} in a flow-through cell. The long-term stability test was performed in 1 M KOH electrolyte at room temperature on a 1×1 cm^2 Ni foam electrode sprayed-coated with an optimized sample loading of 4.5 mg cm^{-2}.

Accordingly, it was proposed that Fe was the active site for the OER and the Ni-LDH acted as a conductive support.[31] Similarly, it was recently found that the inclusion of Fe in Co LDHs improved the OER activity.[20–22,39] Burke et al.[20] attributed the activity improvement to the same synergistic effect as that observed for NiFe LDHs. The Co LDH is assumed to provide a conductive host for Fe, which serves as the (most) active site for the OER.[20] However, unlike the Ni LDHs, Co LDH without Fe exhibits reasonable intrinsic activity for the OER, which emphasizes the potential synergistic effect between Co and Fe as two cooperating active sites.

Recently, by using operando Mössbauer spectroscopy Chen et al.[43] observed that Fe^{4+} was present in the NiFe LDH catalyst during the whole OER-active potential range subsequent to the evolution of oxygen at approximately 1.62 V versus RHE. The role of Fe^{4+} was, however, not fully elucidated in this study, because the presence of Fe^{4+} seemed to be consistent with both the "Ni active site" and the "Fe active site" mechanism. On the other hand, Co^{4+} species have been observed in OER-active catalysts under oxygen evolution conditions and are widely accepted to be a vital intermediate in the OER catalytic cycle by Co-based catalysts.[7,11,44] According to the OER pathway proposed by Ullmann et al.,[45] the Co^{4+} species coordinated to the oxo groups facilitate the proton-coupled electron-transfer (PCET) steps leading to the formation of O$^{\bullet}$ radicals on the Co^{3+} sites. It is well known that Fe is oxidized at a lower potential than Co.[46] Therefore, Fe can substitute Co in the CoFe LDHs in forming oxo species at lower potentials, which may facilitate the PCET steps and ultimately enhance the overall OER catalysis.

Conclusions

Co-based layered double hydroxides (LDHs) were prepared by coprecipitation with Al^{3+} or Fe^{3+} ions. Extensive structural characterization confirmed that the LDH structure was successfully formed with Al^{3+} or Fe^{3+} ions in the range of 15 to 45 at%. Electrochemical studies showed that Al^{3+} suppressed the oxygen evolution reaction (OER) activity, whereas Fe^{3+} enhanced the activity with an optimum content of Fe amounting to 35 at%. The optimal $Co_{0.65}Fe_{0.35}(OH)_2$ catalyst showed very good long-term stability in 1 M KOH for at least 48 h. All results point to a synergistic effect between the Co and Fe ions in the LDH structure, which establishes a systematic basis for further research on Co- and Fe-containing LDHs as catalysts for the OER.

Experimental Section

The catalysts were prepared by coprecipitation by using $Co(NO_3)_2{\cdot}6H_2O$ (Sigma–Aldrich, 99.999%), $Fe(NO_3)_3{\cdot}6H_2O$ (Sigma–Aldrich, 99.999%), $Al(NO_3)_3{\cdot}9H_2O$ (Sigma–Aldrich, 99.997%), NaOH (Sigma–Aldrich, 99.99%), $Na_2CO_3{\cdot}10H_2O$ (Sigma–Aldrich, 99.999%), and HPLC water without any further purification. For a common synthesis, 5 mM $Co(NO_3)_2/Al(NO_3)_3$ or $Co(NO_3)_2/Fe(NO_3)_3$ aqueous solution (10 mL) was dropwise added into water (50 mL) at 25 °C within 30 min under rigorously stirring. At the same time, an alkaline solution containing 2 M NaOH and 0.3 M Na_2CO_3 was added to the solution by using an autotitrator to maintain a pH of 9. After complete addition of the salt solution, the brown suspension was stirred at 25 °C for 2 h. After that, the precipitate was filtered and redispersed in water (3×50 mL). The resulting solid was dried at 30 °C in flowing air overnight and was then finely ground in a mortar for further use.

ICP-OES (PU701 UNICAM) was used to determine the metal content. The XRD patterns were recorded with a Philips X'Pert MPD system with CuK_α irradiation and post-monochromator in the 2θ range of 5 to 80°. The TG measurements were performed by using a Cahn TG 2131 thermobalance coupled with a quadrupole mass spectrometer (QMS, Balzer, Omnistar). Typically, the sample (20 mg) was heated to 800 °C at a rate of 5 °C min^{-1} in 100 mL$_N$ m^{-1} 20 vol% O_2/He flow. The TPR experiments were performed by heating the catalyst (≈50 mg) in a tubular reactor from 50C to 700 °C at a rate of 5 K min^{-1} in a tubular reactor. The H_2 content in the evolved gases was detected by a thermal conductivity detector (Xstream). The Raman spectra were recorded with a diffuse Raman spectrometer (iHR 550, HORIBA) by using the 3.5 mW laser with a wavelength of 532 nm. The XPS measurements were performed in an ultrahigh vacuum setup equipped with a monochromatic AlK_α X-ray source (1486.6 eV; anode operating at 14.5 kV and 35 mA) and a high-resolution Gammadata-Scienta SES 2002 analyzer. The base pressure in the measurement chamber was maintained at approximately 7×10^{-10} mbar. The XP spectra were recorded in the fixed transmission mode with a pass energy of 200 eV. Charging effects were compensated by applying a flood gun. The fitting was performed with a minimum number of peaks by using the CasaXPS software by limiting the peak positions and FWHMs to fixed binding energy ranges. All the XP spectra were calibrated by aliphatic carbon species at a binding energy of 284.5 eV.

The XAFS measurements were performed at the undulator beamline P65 of PETRA III storage ring operating at 6 GeV in top-up mode. The experiments were performed in transmission mode at the Fe*K* (7112 eV) and Co*K* (7709 eV) edges. For each of the samples, multiple identical spectra were acquired and averaged to improve the signal-to-noise ratio. Initial processing of the XAFS data was performed by using the program Athena.[47] EXAFS analysis was conducted in Artemis by using the FEFF8 code[48] to extract

the coordination number (CN), interatomic distance (r), disorder parameter (Debye–Waller factor, σ^2), and edge energy shift, ΔE. The details of the EXAFS analysis are provided in the Supporting Information (Tables S2 and S3).

GC RDE electrodes with a diameter of 3.8 mm were first polished on 1500 grid sand paper and then on a polishing cloth with alumina pastes of different grain sizes (3–0.05 μm), and they were then rinsed in deionized water for 15 min and subsequently in acetone for 5 min. The catalyst ink was prepared by dispersing the catalyst (5 mg), Vulcan XC-72 (1 mg), and 5% Nafion (34 μL) in H_2O/EtOH (1:1, 1 mL) solution. For a given catalyst ink, an aliquot (5.7 μL) was dropped on the electrode and dried at room temperature under rotation at 500 rpm for 15 min. The resulting catalyst loading was 250 $\mu g\,cm^{-2}$. Six electrodes prepared from each ink were tested in a three-electrode system with Pt mesh as a counter electrode and an Orion 900200 Sure-Flow as the reference electrode. The electrolyte was 0.1 M KOH saturated with O_2. Electrochemical impedance spectroscopy (EIS) was measured at the open-circuit potential (OCP) from 500 kHz to 50 Hz with alternating current (AC) perturbation of 10 mV to determine the uncompensated resistance. Linear sweep voltammetry (LSV) was performed between −0.5 and 1.5 V versus Ag/AgCl/3 M KCl reference electrode with a scan rate of 1 $mV\,s^{-1}$ and a rotation rate of 1600 rpm.

Samples for the long-term stability test were deposited on Ni foam electrodes ($1\times1\times0.15\ cm^3$) by means of spray-coating at 120 °C on a hot plate. The catalyst ink contained the catalyst (250 mg), EtOH (28.3 mL), H_2O (20 mL), and 5% Nafion (1.7 mL). The long-term stability test was performed in a flow-through cell controlled by a multichannel biologic VMP-3 potentiostat. The counter electrode was Ni foam ($1\times1\times0.3\ cm^3$), whereas a Ag/AgCl/3 M KCl/1 M KOH double junction electrode served as the reference electrode. For the OER half-cell measurements, the electrolyte (1 M KOH) presaturated by purging with O_2 was continuously pumped from the anolyte electrolyte reservoir through the flow-through cell. A second electrolyte reservoir, containing the catholyte (also 1 M KOH) for the counter reaction (i.e., hydrogen evolution reaction), was presaturated by purging with argon and was pumped through the catholyte compartment of the cell. The anolyte and catholyte cell compartments were separated by a FAAM-75-PK alkaline exchange membrane (FuMA-Tech, Germany) to prevent mixing of H_2 and O_2. EIS was measured at the OCP from 50 kHz to 50 Hz with AC perturbation of 10 mV to determine the uncompensated resistance. Galvanodynamic sweep (GDS) was performed between 0 and 10 mA at a scan rate of 1 $mA\,s^{-1}$ during cycling the electrolyte, followed by chronopotentiometry (CPM) at 10 mA for 30 min. The number of cycles was 96, which corresponded to 48 h of the GSS test.

Acknowledgements

Financial support (SusHy: Grant 03X3581D) from the German Federal Ministry of Education and Research (BMBF) is gratefully acknowledged.

Keywords: cobalt · iron · layered double hydroxides · oxygen evolution reaction · stability

[1] T. R. Cook, D. K. Dogutan, S. Y. Reece, Y. Surendranath, T. S. Teets, D. G. Nocera, *Chem. Rev.* **2010**, *110*, 6474–6502.
[2] M. G. Walter, E. L. Warren, J. R. McKone, S. W. Boettcher, Q. Mi, E. A. Santori, N. S. Lewis, *Chem. Rev.* **2010**, *110*, 6446–6473.
[3] a) N. Danilovic, R. Subbaraman, K.-C. Chang, S. H. Chang, Y. J. Kang, J. Snyder, A. P. Paulikas, D. Strmcnik, Y.-T. Kim, D. Myers, V. R. Stamenkovic, N. M. Markovic, *J. Phys. Chem. Lett.* **2014**, *5*, 2474–2478; b) C. C. L. McCrory, S. Jung, J. C. Peters, T. F. Jaramillo, *J. Am. Chem. Soc.* **2013**, *135*, 16977–16987.
[4] J. Wang, W. Cui, Q. Liu, Z. Xing, A. M. Asiri, X. Sun, *Adv. Mater.* **2016**, *28*, 215–230.
[5] M. W. Kanan, D. G. Nocera, *Science* **2008**, *321*, 1072–1075.
[6] M. Risch, V. Khare, I. Zaharieva, L. Gerencser, P. Chernev, H. Dau, *J. Am. Chem. Soc.* **2009**, *131*, 6936–6937.
[7] J. G. McAlpin, Y. Surendranath, M. Dincă, T. A. Stich, S. A. Stoian, W. H. Casey, D. G. Nocera, R. D. Britt, *J. Am. Chem. Soc.* **2010**, *132*, 6882–6883.
[8] P. Du, O. Kokhan, K. W. Chapman, P. J. Chupas, D. M. Tiede, *J. Am. Chem. Soc.* **2012**, *134*, 11096–11099.
[9] C. L. Farrow, D. K. Bediako, Y. Surendranath, D. G. Nocera, S. J. L. Billinge, *J. Am. Chem. Soc.* **2013**, *135*, 6403–6406.
[10] K. Klingan, F. Ringleb, I. Zaharieva, J. Heidkamp, P. Chernev, D. Gonzalez-Flores, M. Risch, A. Fischer, H. Dau, *ChemSusChem* **2014**, *7*, 1301–1310.
[11] J. B. Gerken, J. G. McAlpin, J. Y. C. Chen, M. L. Rigsby, W. H. Casey, R. D. Britt, S. S. Stahl, *J. Am. Chem. Soc.* **2011**, *133*, 14431–14442.
[12] B. S. Yeo, A. T. Bell, *J. Am. Chem. Soc.* **2011**, *133*, 5587–5593.
[13] J. Bao, X. Zhang, B. Fan, J. Zhang, M. Zhou, W. Yang, X. Hu, H. Wang, B. Pan, Y. Xie, *Angew. Chem. Int. Ed.* **2015**, *54*, 7399–7404; *Angew. Chem.* **2015**, *127*, 7507–7512.
[14] L. Xu, Q. Jiang, Z. Xiao, X. Li, J. Huo, S. Wang, L. Dai, *Angew. Chem. Int. Ed.* **2016**, *55*, 5277–5281; *Angew. Chem.* **2016**, *128*, 5363–5367.
[15] H.-Y. Wang, S.-F. Hung, H.-Y. Chen, T.-S. Chan, H. M. Chen, B. Liu, *J. Am. Chem. Soc.* **2016**, *138*, 36–39.
[16] D. González-Flores, I. Sánchez, I. Zaharieva, K. Klingan, J. Heidkamp, P. Chernev, P. W. Menezes, M. Driess, H. Dau, M. L. Montero, *Angew. Chem. Int. Ed.* **2015**, *54*, 2472–2476; *Angew. Chem.* **2015**, *127*, 2502–2506.
[17] C.-W. Tung, Y.-Y. Hsu, Y.-P. Shen, Y. Zheng, T.-S. Chan, H.-S. Sheu, Y.-C. Cheng, H. M. Chen, *Nat. Commun.* **2015**, *6*, 8106.
[18] K. J. May, C. E. Carlton, K. A. Stoerzinger, M. Risch, J. Suntivich, Y.-L. Lee, A. Grimaud, Y. Shao-Horn, *J. Phys. Chem. Lett.* **2012**, *3*, 3264–3270.
[19] A. Bergmann, E. Martinez-Moreno, D. Teschner, P. Chernev, M. Gliech, J. F. de Araújo, T. Reier, H. Dau, P. Strasser, *Nat. Commun.* **2015**, *6*, 8625.
[20] M. S. Burke, M. G. Kast, L. Trotochaud, A. M. Smith, S. W. Boettcher, *J. Am. Chem. Soc.* **2015**, *137*, 3638–3648.
[21] C. G. Morales-Guio, L. Liardet, X. Hu, *J. Am. Chem. Soc.* **2016**, *138*, 8946–8957.
[22] Y. Vlamidis, E. Scavetta, M. Gazzano, D. Tonelli, *Electrochim. Acta* **2016**, *188*, 653–660.
[23] Z. Liu, R. Ma, M. Osada, K. Takada, T. Sasaki, *J. Am. Chem. Soc.* **2005**, *127*, 13869–13874.
[24] J. Pérez-Ramírez, G. Mul, F. Kapteijn, J. A. Moulijn, *J. Mater. Chem.* **2001**, *11*, 821–830.
[25] J. Yang, H. Liu, W. N. Martens, R. L. Frost, *J. Phys. Chem. C* **2010**, *114*, 111–119.
[26] J. Pérez-Ramírez, G. Mul, J. Moulijn, *Vib. Spectrosc.* **2001**, *27*, 75–88.
[27] S. Velu, K. Suzuki, M. P. Kapoor, S. Tomura, F. Ohashi, T. Osaki, *Chem. Mater.* **2000**, *12*, 719–730.
[28] a) J. A. Díaz, H. Akhavan, A. Romero, A. M. Garcia-Minguillan, R. Romero, A. Giroir-Fendler, J. L. Valverde, *Fuel Process. Technol.* **2014**, *128*, 417–424; b) A. Griboval-Constant, A. Butel, V. V. Ordomsky, P. A. Chernavskii, A. Y. Khodakov, *Appl. Catal. A* **2014**, *481*, 116–126.
[29] A. P. Grosvenor, B. A. Kobe, M. C. Biesinger, N. S. McIntyre, *Surf. Interface Anal.* **2004**, *36*, 1564–1574.
[30] M. Wilke, F. Farges, P.-E. Petit, G. E. Brown, F. Martin, *Am. Mineral.* **2001**, *86*, 714–730.
[31] D. Friebel, M. W. Louie, M. Bajdich, K. E. Sanwald, Y. Cai, A. M. Wise, M.-J. Cheng, D. Sokaras, T.-C. Weng, R. Alonso-Mori, R. C. Davis, J. R. Bargar, J. K. Nørskov, A. Nilsson, A. T. Bell, *J. Am. Chem. Soc.* **2015**, *137*, 1305–1313.
[32] M. Görlin, P. Chernev, J. F. de Araújo, T. Reier, S. Dresp, B. Paul, R. Krähnert, H. Dau, P. Strasser, *J. Am. Chem. Soc.* **2016**, *138*, 5603–5614.
[33] R. W. G. Wyckoff, *Cryst. Struct.* **1963**, 239–444.
[34] a) W. P. Wuelfing, S. J. Green, J. J. Pietron, D. E. Cliffel, R. W. Murray, *J. Am. Chem. Soc.* **2000**, *122*, 11465–11472; b) J. E. Katz, X. Zhang, K. Attenkofer, K. W. Chapman, C. Frandsen, P. Zarzycki, K. M. Rosso, R. W. Falcone, G. A. Waychunas, B. Gilbert, *Science* **2012**, *337*, 1200–1203.

[35] N. Lu, L. Li, W. Banerjee, P. Sun, N. Gao, M. Liu, *J. Appl. Phys.* **2015**, *118*, 45701.
[36] X. Zou, A. Goswami, T. Asefa, *J. Am. Chem. Soc.* **2013**, *135*, 17242 – 17245.
[37] F. Song, X. Hu, *Nat. Commun.* **2014**, *5*, 4477.
[38] F. Song, X. Hu, *J. Am. Chem. Soc.* **2014**, *136*, 16481 – 16484.
[39] B. Zhang, X. Zheng, O. Voznyy, R. Comin, M. Bajdich, M. García-Melchor, L. Han, J. Xu, M. Liu, L. Zheng, F. P. García de Arquer, C. T. Dinh, F. Fan, M. Yuan, E. Yassitepe, N. Chen, T. Regier, P. Liu, Y. Li, P. De Luna, A. Janmohamed, H. L. Xin, H. Yang, A. Vojvodic, E. H. Sargent, *Science* **2016**, *352*, 333 – 337.
[40] A. Maljusch, O. Conradi, S. Hoch, M. Blug, W. Schuhmann, *Anal. Chem.* **2016**, *88*, 7597 – 7602.
[41] L. Trotochaud, S. L. Young, J. K. Ranney, S. W. Boettcher, *J. Am. Chem. Soc.* **2014**, *136*, 6744 – 6753.
[42] L. J. Enman, M. S. Burke, A. S. Batchellor, S. W. Boettcher, *ACS Catal.* **2016**, *6*, 2416 – 2423.
[43] J. Y. C. Chen, L. Dang, H. Liang, W. Bi, J. B. Gerken, S. Jin, E. E. Alp, S. S. Stahl, *J. Am. Chem. Soc.* **2015**, *137*, 15090 – 15093.
[44] M. W. Kanan, J. Yano, Y. Surendranath, M. Dinca, V. K. Yachandra, D. G. Nocera, *J. Am. Chem. Soc.* **2010**, *132*, 13692 – 13701.
[45] A. M. Ullman, C. N. Brodsky, N. Li, S.-L. Zheng, D. G. Nocera, *J. Am. Chem. Soc.* **2016**, *138*, 4229 – 4236.
[46] A. J. Bard, L. R. Faulkner, *Electrochemical Methods: Fundamentals and Applications*, 2nd ed., Wiley, New York, **2001**.
[47] B. Ravel, M. Newville, *J. Synchrotron Radiat.* **2005**, *12*, 537 – 541.
[48] A. L. Ankudinov, B. Ravel, J. J. Rehr, S. D. Conradson, *Phys. Rev. B* **1998**, *58*, 7565 – 7576.

Manuscript received: September 12, 2016
Revised: November 18, 2016
Accepted Article published: November 18, 2016
Final Article published: December 21, 2016